Dominant ion-core assignments for the Rydberg states of Xe_2 dissociating to $Xe+Xe^*(6p,5d)$ by dispersive photoelectron spectroscopy

X. K. Hu, D. M. Mao, S. S. Dimov, and R. H. Lipson*
Department of Chemistry, University of Western Ontario, London, Ontario, Canada N6A 5B7
(Received 14 May 1996)

Dispersive photoelectron spectra and constant-initial- (ionic-) state spectra are presented for the known band systems of jet-cooled Xe_2 that dissociate to $Xe(^1S_0)+Xe^*(6p,5d)$ between approximately 74 627 and 80 849 cm^{-1}. In many instances, the dominant molecular ion-core assignment for each gerade Rydberg state deduced from the photoelectron data agrees well with predictions made from angular momentum arguments. Differences are attributed to either local excited-state homogeneous perturbations or strong predissociation. [S1050-2947(96)02410-9]

PACS number(s): 33.60.−q, 33.20.−t

I. INTRODUCTION

One of the simplest descriptions of a diatomic Rydberg state is that of a molecular ion core plus a nonbonding electron. Consequently, the excited-state potential-energy curve of a given neutral Rydberg level and its associated vibrational and rotational constants are expected to resemble those of the ion core on which the state is built [1].

This concept is a particularly useful starting point for understanding the electronic spectra of the homonuclear rare-gas excimer Xe_2. Its ground state can be adequately represented by the single-configuration closed-shell molecular orbital $...(\sigma_g 5p)^2(\pi_u 5p)^4(\pi_g^* 5p)^4(\sigma_u^* 5p)^2$ [2]. Since the number of bonding and antibonding electrons in the configuration above are equal, the ground state is expected and found to be repulsive except for a shallow van der Waals minimum ($D_e''=196.2$ cm^{-1}) at long bond lengths ($r_e''=4.362$ Å) [3].

In the absence of spin-orbit interactions, each Rydberg state of Xe_2 can be built on one of four possible Xe_2^+ electronic cores $A\ ^2\Sigma^+_{1/2u}$, $B\ ^2\Pi_g$, $C\ ^2\Pi_u$, and $D\ ^2\Sigma^+_{1/2g}$, formed by removing a $\sigma_u^* 5p$, $\pi_g^* 5p$, $\pi_u 5p$, and $\sigma_g 5p$ electron, respectively. Here the state labels are those proposed by Mulliken [4]. Six ion states in total arise when spin-orbit effects are taken into account because each $^2\Pi$ state splits into $^2\Pi_{3/2}$ and $^2\Pi_{1/2}$ components. Although traditionally, Hund's case (a) term symbols have been used for the ion levels, it is anticipated that a Hund's case (c) formalism where the states are labeled by Ω, the component of total angular momentum along the bond axis, is better [5].

At short internuclear separations, the ionic levels, in order of increasing energy, are $A\ ^2\Sigma^+_{1/2u}$, $B\ ^2\Pi_{3/2g}$, $B\ ^2\Pi_{1/2g}$, $C\ ^2\Pi_{3/2u}$, $C\ ^2\Pi_{1/2u}$, and $D\ ^2\Sigma^+_{1/2g}$. However, the potential-energy curves of $B\ ^2\Pi_{1/2g}$ and $C\ ^2\Pi_{3/2u}$ are predicted to cross each other near $r\approx 3.3$ Å, thereby reversing the energy ordering of those two states at longer bond lengths [6–8]. The relative magnitudes of the dissociation energies of the ionic states, D_e^i, based on their molecular-orbital descriptions, are expected to be $D_e^i(A)\gg D_e^i(B)>D_e^i(C)>D_e^i(D)$. Departures from this picture arise because of the spin-orbit interaction that mixes $C\ ^2\Pi_{1/2u}$ with $A\ ^2\Sigma^+_{1/2u}$ giving the former more bound character than expected, and $B\ ^2\Pi_{1/2g}$ with $D\ ^2\Sigma^+_{1/2g}$, making that B state quite repulsive.

Correlating each neutral Xe_2 Rydberg state with a specific ion core can be done by first considering the electronic structure of Xe_2^+ in the separated atom-ion limit. Each molecular ion state is derived from a ground-state Xe-atom–Xe^+-ion combination. The $Xe^+\ ^2P^o$ ground state is split by the spin-orbit interaction into $^2P^o_{3/2}$, and $^2P^o_{1/2}$ components separated by 10 537.0 cm^{-1} [9]. The $A\ ^2\Sigma^+_{1/2u}$, $B\ ^2\Pi_{3/2g}$, $B\ ^2\Pi_{1/2g}$, and $C\ ^2\Pi_{3/2u}$ ion states result from $Xe(^1S_0)+Xe^+(^2P^o_{3/2})$, while $C\ ^2\Pi_{1/2u}$ and $D\ ^2\Sigma^+_{1/2g}$ are formed from $Xe(^1S_0)+Xe^+(^2P^o_{1/2})$.

In this paper, transitions involving Xe_2 gerade Rydberg states that yield $Xe(^1S_0)+Xe^*(6p,6d)$ at dissociation will be discussed. Since each excited asymptotic atomic term under consideration is built upon $Xe^+(^2P^o_{3/2})$ [9], only the $A\ ^2\Sigma^+_{1/2u}$, $B\ ^2\Pi_{3/2g}$, $B\ ^2\Pi_{1/2g}$, and $C\ ^2\Pi_{3/2u}$ molecular ion cores need to be considered. These can be further distinguished because the parity of the orbital angular momentum l is odd and even for a p and d Rydberg electron, respectively. Thus the gerade Rydberg states dissociating to $Xe(^1S_0)+Xe^*(6p)$ will be built on the $A\ ^2\Sigma^+_{1/2u}$ and $C\ ^2\Pi_{3/2u}$ cores, while those dissociating to $Xe(^1S_0)+Xe^*(5d)$ will be derived from $B\ ^2\Pi_{3/2g}$ and $B\ ^2\Pi_{1/2g}$.

The most straightforward means of determining the electronic structure of any molecule is through the interpretation of electronic spectra. The lowest-lying Rydberg states dissociating to $Xe(^1S_0)+Xe^*(6p,5d)$ are now well characterized from the experiments of Lipson and co-workers, who used (2+1) resonantly enhanced multiphoton ionization (REMPI) in conjunction with time-of-flight (TOF) mass detection and polarization measurements to derive excited-state electronic symmetries and vibrational constants [10–12]. It was found that the experimentally determined dissociation energies D_e' and vibrational frequencies ω_e' could be rationalized through comparisons of like parameters for the ion cores *predicted* to be associated with each state in question [12].

In principle, photoelectron spectroscopy (PES) can pro-

*Author to whom correspondence should be addressed. Electronic address: rlipson@uwovax.uwo.ca

 © 1996 The American Physical Society

vide direct unambiguous *proof* of the identity of the ion core associated with a particular Rydberg level. Xe_2^+ has been studied by a number of different photoelectron techniques including dispersive PES using He (I) light sources [13,14], laser REMPI-PES [15], and threshold PES [16–19]. In fact, the $A\ ^2\Sigma^+_{1/2u}$, $B\ ^2\Pi_{3/2g}$, $C\ ^2\Pi_{3/2u}$, $C\ ^2\Pi_{1/2u}$, and $D\ ^2\Sigma^+_{1/2g}$ ion states are now known to vibrational precision due to the latter experiments.

Despite the impressive high-frequency resolution possible with threshold PES, dispersive PES provides useful information that offsets its lower resolution when used in combination with REMPI. If the interaction between the ion core associated with the intermediate excited state and the Rydberg electron is weak, ionization will usually preserve the ion-core electronic state [20].

In addition, the photoelectron (PE) spectrum of a perturbed level reflects the character of all neutral states involved in the interaction [21]. This is particularly important here since interstate couplings are expected between Xe_2 levels of the same symmetry [22]. In this paper, dispersive PES has been used to provide dominant ion-core identities for the Rydberg states of Xe_2 dissociating to $Xe(^1S_0)+Xe^*(6p,5d)$. In most instances and where possible, the results compare favorably with the literature [15] and with predictions made previously from angular momentum arguments [12].

II. EXPERIMENT

Detailed descriptions of the REMPI-TOF mass spectrometer have been provided elsewhere [10,23]. The ultraviolet (uv) fundamental wavelengths required to excite two-photon transitions from the ground state of Xe_2 to the excited Rydberg states of interest between approximately 76 900 and 80 100 cm^{-1} were generated in this experiment by frequency doubling the output a Nd:YAG-pumped dye laser (where YAG denotes yttrium aluminum garnet) operating on a Coumarin 500/methanol solution in a β-barium-borate (BBO) crystal (Inrad Autotraker II).

Xe_2 excimers were produced by expanding an approximately 20% Xe in He mixture [stagnation pressure approximately equal to 115 psi (absolute)] in a pulsed (approximately 130 μsec) supersonic jet at a repetition rate of 10 Hz. The pressure inside the vacuum chamber rose from the base level of less than or equal to 10^{-6} Torr to approximately 8×10^{-5} Torr when the valve was operating. The uv light was focused with a $f=84$ cm quartz lens approximately 20 mm below the 1.0-mm-diam pinhole of the valve located between the grids of the linear TOF mass spectrometer (Comstock TOF-101).

Photoelectron kinetic energies were measured using a double focusing electrostatic energy analyzer (36.5 mm mean radius, Comstock, Model AC-901) whose entrance was located 180° to the axis of the flight tube of the TOF mass spectrometer and horizontally approximately 5 mm from the focus of uv laser beam in the jet. The device was placed inside a magnetic shield box made of μ metal and held rigidly in place with an insulated aluminum bracket mounted to the flight tube. The inside of the spectrometer was sprayed with a colloidal graphite suspension to minimize patch contact potentials. Since the back repeller plate of the TOF mass spectrometer is made of mesh, it was not removed for these measurements. However, the grids and flight tube were grounded to eliminate stray electric fields that could have developed through charging.

Photoelectrons produced by the (2+1) REMPI process and moving within the acceptance angle of the spectrometer (0.002 sr) were focused into its 2-mm-diam entrance hole with a custom-made three-plate Einzel lens (Comstock) whose third element was the analyzer entrance plate itself. An 18-mm-diam dual microchannel plate mounted at the exit of the spectrometer (Comstock Model MCP-602B) was used for detection.

All voltages required to bias the photoelectron spectrometer were obtained from a power supply accompanying the device (Comstock, Model ES-101). The ramping voltage from the power supply, used to smoothly change the transmission energy of the spectrometer, was controlled externally with a multichannel scaling and control card (Comstock, Model MCS-702). Typically, the voltage was continuously ramped 5 V in approximately 3.4 min, corresponding to a rate of 0.0244 V/sec. The microchannel plate detector output was preamplified and (30 point) averaged in a gated integrator-boxcar averager (SRS, Model SR250) and both the photoelectron signals and ramping voltage were digitized at the same time (SRS interface, model SR245) and stored in a XT computer for later analysis.

The experimentally determined kinetic-energy full width at half maximum $\Delta E=172$ meV of an isolated atomic photoelectron peak at 5 eV pass energy is in reasonable agreement with the theoretical estimate of 137 meV. While, in principle, the resolving power of the spectrometer could have been increased by at least a factor of 2 using a smaller aperture, the photoelectron signals were found to be too weak to be measured under those experimental conditions. Tests showed that the energy resolution in the photoelectron spectra under our experimental conditions was not affected by space-charge formation, the magnetic field of the pulsed valve, or the background gas pressure in the vacuum chamber.

III. RESULTS AND ANALYSIS

Dispersive PES experiments were carried out for the six regions of Xe_2 described previously [10,11]. Overview (2+1) REMPI-TOF spectra obtained using linearly and circularly polarized uv fundamentals, respectively, can be inspected in Fig. 1 of Ref. [11]. Repeated here for the benefit of the discussion below is a diagram (Fig. 1) correlating the states formed by the addition of a $6p\sigma$ and $6p\pi$ Rydberg electron to the A and C cores of Xe_2^+ to those obtained in the separated atom limit [12]. Similarly, Fig. 2 was constructed by considering the addition of a $5d\sigma$, $5d\pi$, and $5d\delta$ Rydberg electron to the two molecular ion B cores [12]. The Ω symmetries on the left-hand side of each correlation diagram were deduced by adding together the appropriate components of the total angular momenta of the Rydberg electron ω_j and the ion core $\Omega_{\rm core}$ [5]. The drawings were made by assuming that the $\Omega_{\rm core}$ energy splittings are smaller than the ω_j intervals. The value of Figs. 1 and 2 is that they predict the ion core of each Ω electronic state associated with a particular asymptotic limit provided that interstate pertur-

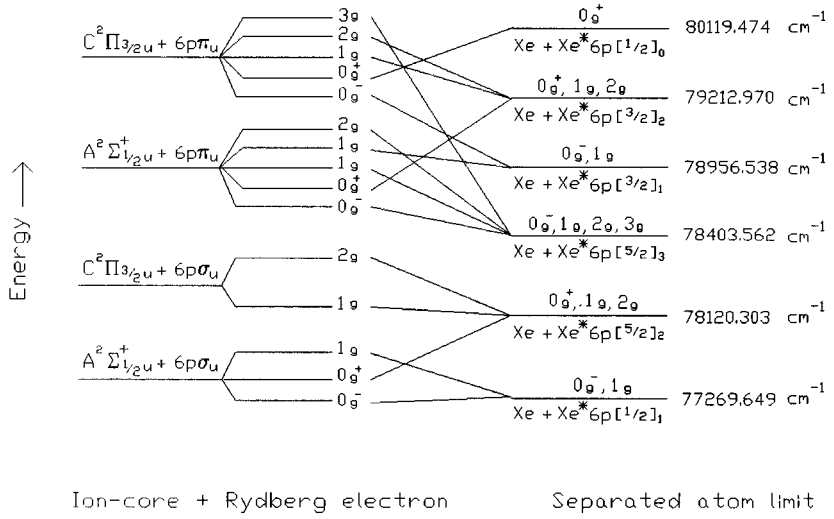

FIG. 1. Correlation diagram for the gerade excited states of Xe_2 dissociating to $Xe(^1S_0)+Xe^*(6p)$. All neutral excimer excited states are labeled in Hund's case (c) nomenclature. The vertical axes on the left- and right-hand sides of the figure are not to scale or equal to one another. The case (c) state splittings on the left-hand side (ion core plus Rydberg electron) combinations are there for visual clarity only. The figure was drawn by assuming that the ion-core state splittings are less than the separations between the ω_j components of the Rydberg electron.

bations can be ignored. As mentioned above, however, both *ab initio* calculations [24,25] and some of the results below indicate that this assumption may not always be a good one.

Two different types of photoelectron spectra were recorded in each spectral region for this study. In the first and more common presentation, the photoemitted electrons were measured as a function of kinetic energy for a single-laser REMPI transition. This will be referred to simply as a PE spectrum, and a summary of our results derived from such data by spectral region is given in Table I. The second approach involved fixing the photoelectron spectrometer pass energy and scanning the laser frequency to obtain a ''constant-initial-state'' [26] or ''constant-ionic-state'' [27,28] (CIS) spectrum.

A. Region I

Region I of the (2+1) REMPI-TOF spectrum of Xe_2 is dominated by a single $0_g^+ \leftarrow 0_g^+$ transition whose excited state dissociates to $Xe(^1S_0)+Xe^*6p[1/2]_0$. The following procedure was followed here for data acquisition (and for the other sections below): First, one set of five PE spectra for the closest atomic Xe transition was measured for calibration purposes, followed by one or two sets of five scans for the molecular system of interest. This sequence was then repeated. The experiment concluded with a final set of five atomic PE spectra.

A typical PE spectrum for the Xe* $6p[1/2]_0 \leftarrow Xe(^1S_0)$ transition in region I at 80 119.474 cm^{-1} [9] is presented in Fig. 3. Although the excited atomic term was expected to produce only a $Xe^+(^2P^o_{3/2})$ photoelectron peak, the higher-energy $Xe^+(^2P^o_{1/2})$ spin-orbit component is also present. A similar observation was noted in published studies of the (3+2) multiphoton ionization of Xe via the $6s[3/2]^o_1$ excited state, which is also built on $Xe^+(^2P^o_{3/2})$ [29,30]. There it was found that the core admixture is introduced at the four-photon energy by states of the $6p'$ manifold. However, the angular distribution of the $6s[3/2]^o_1$ photoelectrons is also

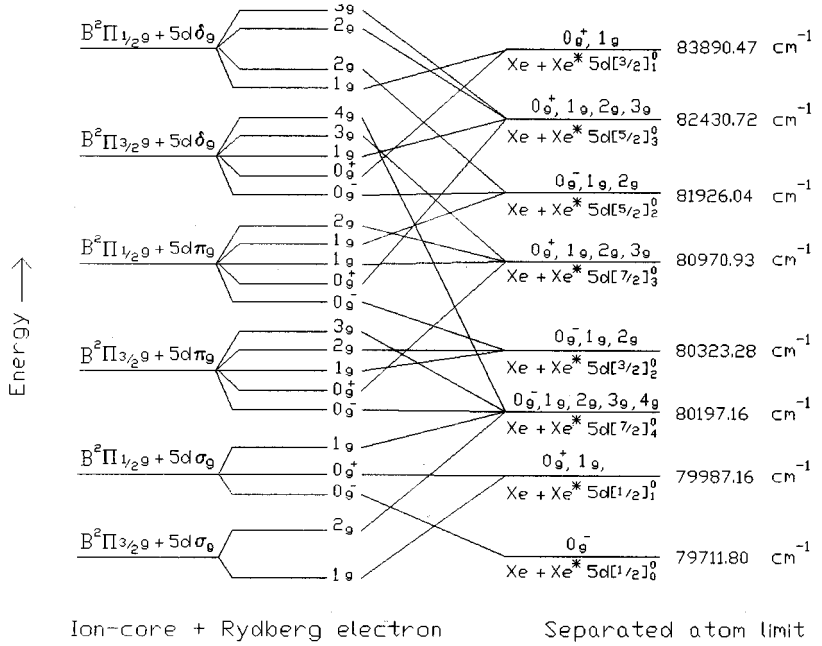

FIG. 2. Correlation diagram for the gerade excited states of Xe_2 dissociating to $Xe(^1S_0)+Xe^*(5d)$. The description given in the caption for Fig. 1 pertains to this drawing as well.

TABLE I. Transitions, photoelectron kinetic energies (P_{KE}), and dominant core assignments for the Rydberg states of Xe_2 dissociating to $Xe(^1S_0)+Xe^*(6p,5d)$.

Region	Transition	Wave number (cm^{-1})	KE (eV)	Dominant core assignment
I	$0_g^+(v'=0)\leftarrow 0_g^+(v''=0)$	80 046	2.83	$Xe_2^+(C\ ^2\Pi_{3/2u})$[a]
			1.52	
II	$0_g^+(v'=0)\leftarrow 0_g^+(v''=0)$	79 611	2.77	$Xe_2^+(C\ ^2\Pi_{3/2u})$[a]
			1.50	
	$1_g(v'=9)\leftarrow 0_g^+(v''=0)$	79 488	2.62	$Xe^+(^2P^o_{3/2})$[b]
	$1_g(v'=7)\leftarrow 0_g^+(v''=0)$	77 378	2.48	$Xe^+(^2P^o_{3/2})$[c]
III	$2_g(v'=4)\leftarrow 0_g^+(v''=0)$	78 978	2.71	$Xe_2^+(C\ ^2\Pi_{3/2u})$
			2.53	$Xe_2^+(B\ ^2\Pi_{3/2g})$[d]
	$1_g(v'=26)\leftarrow 0_g^+(v''=0)$	78 868	2.47	$Xe^+(^2P^o_{3/2})$[e]
IV	$2_g(v'=0)\leftarrow 0_g^+(v''=0)$	78 016	2.47	$Xe_2^+(C\ ^2\Pi_{3/2u})$[a]
V	$0_g^+(v'=32)\leftarrow 0_g^+(v''=0)$	77 587	3.12	$Xe_2^+(A\ ^2\Sigma^+_{1/2u})$
VI	$1_g(v'=43)\leftarrow 0_g^+(v''=0)$	77 017	3.10	$Xe_2^+(A\ ^2\Sigma^+_{1/2u})$[a]

[a]Perturbed.
[b]Predissociation to produce $Xe^*6p[3/2]_2$.
[c]Predissociation to produce $Xe^*6p[5/2]_2$.
[d]Perturber photoelectron peak.
[e]Predissociation to produce $Xe^*6p[5/2]_3$.

sensitive to the degree of $6s$-$5d$ mixing [31,32]. By analogy, the ''purity'' of the Xe* $6p[1/2]_0$ atomic state being considered in this work could also be degraded through interactions with atomic levels having the $^2P^o_{1/2}$ core. Although $6s'$ and $6p'$ $J=0$ states are closest energywise, a complete understanding of the spectrum will invariably require multichannel quantum-defect theory [33].

The average measured ground-state spin-orbit splitting of approximately 10 579(100) cm^{-1} from the atomic ion spectra obtained with our system is in excellent agreement with the literature value of 10 537 cm^{-1} [9]. Sometimes, however, the absolute electron kinetic energies measured for each spin-orbit peak were found to drift slightly due to changing contact potentials within the spectrometer ($\leqslant 3\times10^{-4}$ eV/min). Then the time was noted when each set of atomic and molecular PE spectra was recorded. The atomic photoelectron kinetic-energy drift for the $Xe^+(^2P^o_{3/2})$ spin-orbit component relative to the expected (calculated) theoretical value was subsequently plotted as a function of time, and the best linear fit of these data was used to correct the peak molecular photoelectron energies by interpolation.

The molecular PE spectrum in region I is shown in Fig. 4(a). The uv laser was tuned to excite the $(v',v'')=(0,0)$ two-photon transition of the band system at approximately 80 046 cm^{-1} [10]. Two photoelectron peaks are evident at 1.52 and 2.83 eV, respectively.

Consider the higher-energy feature first. Photoelectrons are believed to be produced by direct ionization since three

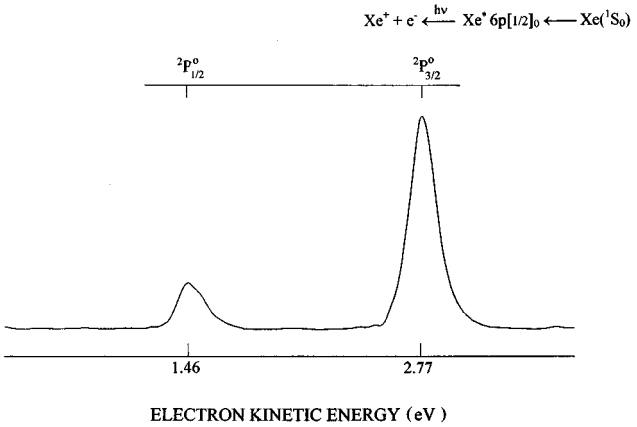

FIG. 3. Photoelectron spectrum for the Xe $6p[1/2]_0\leftarrow Xe(^1S_0)$ two-photon transition at 80 119.474 cm^{-1}.

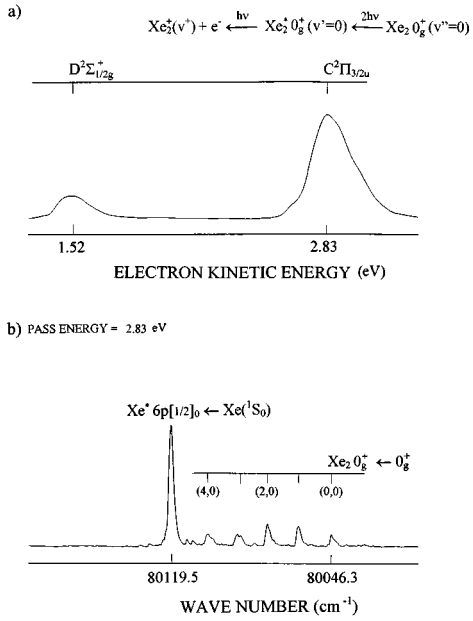

FIG. 4. (a) PE spectrum for the Xe_2 $0_g^+(v'=0)\leftarrow 0_g^+(v'=0)$ two-photon transition at approximately 80 046 cm^{-1} in region I. (b) Constant-initial (ionic) -state spectrum obtained by setting the pass energy of the photoelectron spectrometer to 2.83 eV and frequency scanning the uv laser. Vibrational assignments for the Xe_2 $0_g^+\leftarrow 0_g^+$ two-photon transitions are those reported in Ref. [10].

photons of the uv fundamental beam ($\lambda \approx 249.86$ nm), having a total energy of approximately 120 069 cm^{-1}, exceeds the $Xe + Xe^+(^2P^0_{1/2})$ production threshold at 108 371.4 cm^{-1} [9]. Given that the (2+1) REMPI process can be viewed as a single-step ionic transition originating from a specific vibrational level v' of the 0^+_g Rydberg state, the probability P of accessing a particular vibronic state v^+ of Xe_2^+ should be well approximated by

$$P \alpha \langle \psi_e^+ | \mu | \psi_e' \rangle |\langle \psi_{v^+} | \psi_{v'} \rangle|^2, \quad (1)$$

where $\langle \psi_e^+ | \mu | \psi_e' \rangle$ is the electric-dipole matrix element connecting the Rydberg and molecular ion electronic states and $|\langle \psi_{v^+} | \psi_{v'} \rangle|^2$ is the vibrational Franck-Condon factor [34]. As in conventional optical spectroscopy, the latter quantity governs the relative intensities of the resultant vibronic transitions.

The kinetic energies of the photoelectrons P_{KE}, generated by the (2+1) REMPI process using a fundamental laser beam of frequency ν, is given by

$$P_{KE} \approx 3h\nu - [A_{IP} + G(v^+)], \quad (2)$$

where A_{IP} is the adiabatic ionization potential of a particular Xe_2^+ electronic state and $G(v^+)$ is the vibrational term value of the excited ion core in a level v^+ corresponding to the largest Franck-Condon factor for the transition originating from v' of the neutral Rydberg state. Together, $[A_{IP} + G(v^+)]$ represents the vertical ionization potential.

As noted before, the 0^+_g state in region I can be built only on Xe_2^+ $A\ ^2\Sigma^+_{1/2}$ or $C\ ^2\Pi_{3/2u}$. Therefore, Franck-Condon calculations using Morse-Rydberg-Klein-Rees potential-energy curves [35] for the Rydberg state and each ion core were carried out separately in the same manner as that described elsewhere [36] to establish the Xe_2^+ state assignment for the observed photoelectron peak.

The vibrational frequency ω_e', anharmonicity $\omega_e x_e'$, and equilibrium bond length r_e' of the 0^+_g Rydberg state for the most abundant isotopomer $^{129}Xe^{132}Xe$ were determined from (2+1) REMPI-TOF mass spectrometry and Franck-Condon calculations to be 18.66(31) cm^{-1}, 0.273(81) cm^{-1}, and 4.59 Å, respectively [10,11]. The vibrational constants for the molecular ion A state, $\omega_e^+ = 123.4$ cm^{-1} and $\omega_e x_e^+ = 0.484$ cm^{-1}, are those reported in a synchrotron threshold PES study [19]. That work also provided $A_{IP} = 90\,139.7$ cm^{-1}. The A-state equilibrium bond length used was the theoretical value of $r_e^+ = 3.17$ Å calculated by Daskalopoulou, Böhmer, and Peyerimhoff [8]. The Xe_2^+ $C\ ^2\Pi_{3/2u}$ constants $\omega_e^+ = 23.1$ cm^{-1}, $\omega_e x_e^+ = 0.55$ cm^{-1}, $A_{IP} = 97\,576(2)$ cm^{-1}, and $r_e^+ = 4.27$ Å were obtained by Tonkyn and White from a single-photon threshold PES study using coherent, monochromatic vacuum ultraviolet radiation generated by frequency tripling in argon gas [16].

The largest Franck-Condon factors for the Xe_2^+ $A\ ^2\Sigma^+_{1/2u}(v^+) \leftarrow Xe_2^*$ $0^+_g(v'=0)$ and Xe_2^+ $C\ ^2\Pi_{3/2u} \leftarrow Xe_2^+$ $0^+_g(v'=0)$ transitions were found for $v^+ = 62$ and 0, respectively, corresponding to $G_A(v^+ = 62) = 5821.9$ cm^{-1} and $G_c(v^+ = 1) = 33.4$ cm^{-1}. Substituting these numbers and the data above into Eq. (2) yields calculated photoelectron kinetic energies of 2.99 eV for the $A\ ^2\Sigma^+_{1/2u} \leftarrow 0^+_g$ transition and 2.78 eV for $C\ ^2\Pi_{3/2u} \leftarrow 0^+_g$. The former result differs from the experimentally determined value by 0.14 eV, while the latter lies within 0.07 eV. Given that the experimental measurement error is on the order of approximately 0.03 eV and that the level is perturbed by a lower-lying 0^+_g state that dissociates to $Xe(^1S_0) + Xe^*\ 5d[1/2]^o_1$ and is built on the $B\ ^2\Pi_{1/2g}$ core, it can be concluded that the 0^+_g Rydberg state in region I is built on the $C\ ^2\Pi_{3/2u}$ ion core, in agreement with the correlation diagram in Fig. 1.

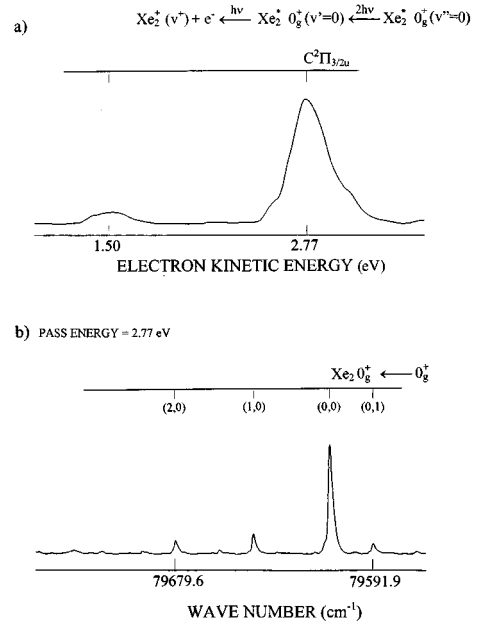

FIG. 5. (a) PE spectrum for the Xe_2 $0^+_g(v'=0) \leftarrow 0^+_g(v'=0)$ two-photon transition at approximately 79 611 cm^{-1} in region II. (b) CIS spectrum obtained by setting the pass energy of the photoelectron spectrometer to 2.77 eV and frequency scanning the uv laser. Vibrational assignments for the Xe_2 $0^+_g \leftarrow 0^+_g$ two-photon transitions are those reported in Ref. [10].

Figure 4(b) is the CIS spectrum obtained by fixing the photoelectron spectrometer pass energy to the peak kinetic energy of the strongest feature in Fig. 4(a). The appearance of the resultant mass-unresolved excitation spectrum of Xe_2 is in good agreement with previous studies [10,11].

The lower-kinetic-energy feature in Fig. 4(a) at 1.52 eV corresponds well to the formation of Xe_2^+ in the $D\ ^2\Sigma^+_{1/2g}$ excited state. However, the peak is also problematic in that there are two possible explanations for its origin. The first is that the neutral Xe_2 excited state in question interacts with another molecular level having the D ion core or that the mixed nature of the Xe* $6p[1/2]_0$ atomic term is carried over into the molecular photoelectron spectrum. Since the relative intensities of the two photoelectron peaks in Figs. 3 and 4(a) are similar, we favor the second scenario. Still, more work on this issue is required.

B. Region II

There are two band systems in region II involving 0^+_g and 1_g excited states that dissociate to $Xe(^1S_0) + Xe^*\ 5d[1/2]^o_1$ [10–12].

1. The 0^+_g Rydberg state

When the $0^+_g(v'=0) \leftarrow 0^+_g(v''=0)$ two-photon transition at approximately 79 611 cm^{-1} was excited two features

at 1.50 and 2.77 eV were measured from the resultant PE spectrum [Fig. 5(a)]. The molecular kinetic energies were calibrated against PE spectra for the Xe* $6p[1/2]_0 \leftarrow \mathrm{Xe}(^1S_0)$ two-photon transition.

By symmetry, the Xe_2 Rydberg state can be built on either the Xe_2^+ $B\ ^2\Pi_{3/2g}$ or $B\ ^2\Pi_{1/2g}$ ion cores. Franck-Condon calculations were carried out using the $B\ ^2\Pi_{3/2g}$ molecular constants determined by Hall *et al.*: $A_{\mathrm{IP}}=96\,229.12\ \mathrm{cm}^{-1}$, $\omega_e^+=58.39\ \mathrm{cm}^{-1}$, and $\omega_e x_e^+=0.484\ \mathrm{cm}^{-1}$ [19]. The calculated bond length of $r_e^+=3.91$ Å was used for the ionic equilibrium internuclear separation [8]. Since the $B\ ^2\Pi_{1/2g}$ ion core is predicted to be essentially repulsive, a lower limit for its vertical ionization potential I_P was taken to be the energy of the $\mathrm{Xe}(^1S_0)+\mathrm{Xe}^+(^2P^o_{3/2})$ asymptote at 97 834.4 cm^{-1} [9].

The largest Franck-Condon factor for the Xe_2^+ $B\ ^2\Pi_{3/2g}(v^+)\leftarrow \mathrm{Xe}_2^*\ \ 0_g^+(v'=0)$ transition occurs for $v^+=3$. The resultant photoelectron kinetic energy is therefore calculated to be 2.85 eV. Similarly, the calculated photoelectron energy for the Xe_2^+ $B\ ^2\Pi_{1/2g}\leftarrow \mathrm{Xe}_2^*\ 0_g^+(v'=0)$ transition is found to be less than or equal to 2.68 eV. It can be seen that the measured value of 2.77 eV lies almost halfway between the two predictions. Although the Rydberg state is expected to have the repulsive $B\ ^2\Pi_{1/2g}$ ion core (Fig. 2), we had previously postulated that its binding energy ($D_e'=579.4\ \mathrm{cm}^{-1}$) was a result of a homogeneous interaction with the 0_g^+ state in region I built on the C core [12]. When a subsequent Franck-Condon factor calculation was carried out using the $C\ ^2\Pi_{3/2u}$ ion-state potential-energy curve, the photoelectron energy was predicted to be $P_{\mathrm{KE}}=2.71$ eV. This lies closer to our observation and suggests that $C\ ^2\Pi_{3/2u}$ is the dominant core of the 0_g^+ state in this region due to perturbations.

Interestingly, the same conclusion was reached by Dehmer, Pratt, and Dehmer, who also used dispersive PES to study the same vibronic transition [15]. However, more structure is resolved in their spectrum. They assigned the strongest feature at $P_{\mathrm{KE}}\approx 2.7$ eV to $C\ ^2\Pi_{3/2u}$ ion core and a slightly weaker peak in their spectrum at $P_{\mathrm{KE}}\approx 2.8$ eV to $B\ ^2\Pi_{3/2g}$. The latter energy agrees with our Franck-Condon analysis above, but its origin is uncertain. One possible explanation is that the 0_g^+ state in region II also interacts with a second Rydberg state having the $B\ ^2\Pi_{3/2g}$ core. From Fig. 2, the only 0_g^+ state that is likely to be involved energywise dissociates to $\mathrm{Xe}(^1S_0)+\mathrm{Xe}^*\ 5d[7/2]^o_3$ at 80 970.93 cm^{-1} [9].

The CIS scan in Fig. 5(b), obtained by setting the pass energy of the spectrometer to 2.77 eV, reproduces the well-known (2+1) REMPI spectrum [10]. As is the case in region I, the weaker photoelectron band at 1.50 eV in Fig. 5(a) is difficult to explain, even though it was observed before by Dehmer, Pratt, and Dehmer [15]. Since the Xe* $5d[1/2]^o_1 \leftarrow \mathrm{Xe}(^1S_0)$ transition is two-photon electric-dipole forbidden, the core nature of the atomic excited state and its relationship to the molecular spectrum must remain an open question.

2. The 1_g Rydberg state

The PE spectrum obtained by exciting the (9,0) band of the Xe_2 $1_g \leftarrow 0_g^+$ two-photon transition near 79 488 cm^{-1} is shown in Fig. 6(a). The single photoelectron peak comes at 2.62 eV. This result is in poor agreement with $P_{\mathrm{KE}}=2.83$ eV obtained from Franck-Condon factor calculations made by

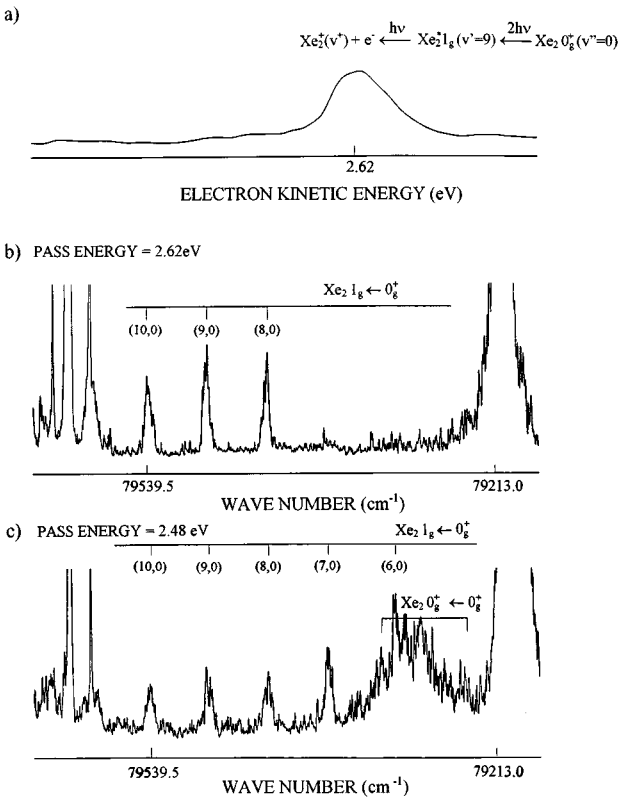

FIG. 6. (a) PE spectrum for the Xe_2 $1_g(v'=9)\leftarrow 0_g^+(v'=0)$ two-photon transition at approximately 79 488 cm^{-1} in region II. (b) CIS spectrum obtained by setting the pass energy of the photoelectron spectrometer to 2.62 eV and frequency scanning the uv laser. Vibrational assignments for the Xe_2 $1_g \leftarrow 0_g^+$ two-photon transitions are those reported in Ref. [12]. The intense feature near 79 213 cm^{-1} is the atomic Xe* $6p[3/2]_2 \leftarrow \mathrm{Xe}(^1S_0)$ two-photon transition, while the strong features on the left-hand side are the molecular bands shown in Fig. 5(b). (c) CIS spectrum obtained by setting the pass energy of the photoelectron spectrometer to 2.48 eV and frequency scanning the uv laser. In addition to finding more (low v',0) transitions of the Xe_2 $1_g \leftarrow 0_g^+$ two-photon transition noted in (b), a broad unresolved feature to the blue of the Xe* $6p[3/2]_2 \leftarrow \mathrm{Xe}(^1S_0)$ transition is evident, which has been tentatively assigned to a Xe_2 $0_g^+ \leftarrow 0_g^+$ transition whose excited state dissociates to Xe* $6p[3/2]_2+\mathrm{Xe}(^1S_0)$.

assuming that the 1_g Rydberg state is built upon the $B\ ^2\Pi_{3/2g}$ ion core, as predicted by the correlation diagram in Fig. 2.

An alternate interpretation can be made by noting that a reasonably strong (2+1) REMPI spectrum could only be attained for the $1_g \leftarrow 0_g^+$ transition in region II by monitoring atomic Xe^+ in TOF detection. This is indicative of a strongly predissociated excited state. Consequently, the photoelectrons most likely originate from an excited Xe term that is produced by rapid predissociation, that is, $\mathrm{Xe}_2+2h\nu \rightarrow \mathrm{Xe}_2^*+\mathrm{Xe}^*+\mathrm{Xe}+h\nu \rightarrow \mathrm{Xe}^+ + e^- + \mathrm{Xe}$. The electron energies possible from the process above can be calculated from

$$P_{\mathrm{KE}}=\nu(\mathrm{Xe}^*)+h\nu-I_P(\mathrm{Xe}^+\ ^2P^o_{3/2}), \tag{3}$$

where $\nu(\mathrm{Xe}^*)$ the energy of a specific excited atomic Xe term and $h\nu$ is the fundamental single-photon laser energy used to excite the molecular two-photon transition. Excellent

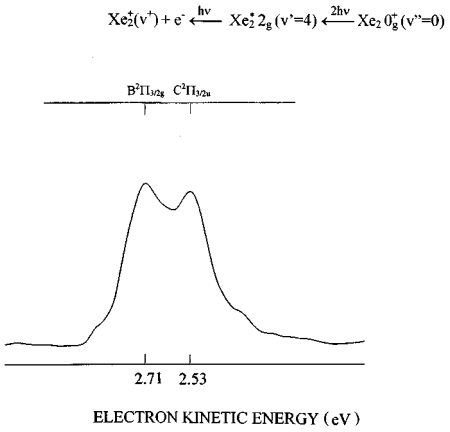

FIG. 7. PE spectrum for the Xe_2 $2_g(v'=4) \leftarrow 0_g^+(v'=0)$ two-photon transition at 78 977.8 cm^{-1} in region III.

agreement is obtained between the experimental measurement and Eq. (3) if the predissociation product is Xe* $6p[3/2]_2$ at 79 212.970 cm^{-1} [9].

The CIS spectrum, obtained with a constant pass energy of 2.62 eV and displayed in Fig. 6(b), exhibits the strongest bands of the $1_g \leftarrow 0_g^+$ transition, as expected [12]. Interestingly, when the (7,0) band of the same system was excited near 77 377.5 cm^{-1} the resultant photoelectron kinetic energy was found to be 2.48 eV. The CIS spectrum obtained with this substantially lower pass energy [Fig. 6(c)] shows that the bands of the $1_g \leftarrow 0_g^+$ transition with $v' < 7$ are stronger, as well as a previously unassigned broad unresolved envelope just to the blue of the Xe* $6p[3/2]_2$ resonance line. A careful reexamination of our (2+1) REMPI-TOF spectra recorded with circularly polarized light [12] supports a 0_g^+ symmetry assignment for the latter feature.

The only 0_g^+ state in the immediate vicinity that has not been accounted for dissociates to $Xe(^1S_0)$+Xe* $6p[3/2]_2$. Once again the photoelectrons are also thought to originate from an excited Xe term produced by strong predissociation. Excellent agreement is found between the experimental measurement and Eq. (3) using ν(Xe* $6p[5/2]_2$)=78 120.303 cm^{-1} [9]. Since different kinetic energies are required to produce Figs. 6(b) and 6(c) it can be inferred that more than one v'-dependent channel of predissociation exists for the 1_g state in region II.

The only problem with our interpretation is that the correlation diagram in Fig. 1 predicts that both 0_g^+ states dissociating to $Xe(^1S_0)$+Xe* $6p[3/2]_2$ and $Xe(^1S_0)$+Xe* $6p[5/2]_2$, respectively, are built on the deeply bound A core. It may be that the potential-energy curve of the 0_g^+ state involved in Fig. 6(c) has a hump that supports levels above its dissociation limit. *Ab initio* calculations in this regard would be invaluable.

C. Region III

Two interleaved $2_g \leftarrow 0_g^+$ and $1_g \leftarrow 0_g^+$ transitions are found in region III and both excited states are thought to dissociate to $Xe(^1S_0)$+Xe* $6p[3/2]_2$ [11,37]. All molecular photoelectron kinetic energies were calibrated against PE spectra recorded for the Xe* $6p[3/2]_2 \leftarrow Xe(^1S_0)$ transition at 79 212.970 cm^{-1}.

1. The 2_g Rydberg state

The excited 2_g state in region III is relatively shallow (D_e=596.2 cm^{-1}) and is strongly predissociated for v' levels greater than 5. The PE spectrum shown in Fig. 7, obtained by exciting the (4,0) band at 78 977.8 cm^{-1}, is a closely spaced doublet with maxima corresponding to P_{KE}=2.53 and 2.71 eV, respectively. Using the known 2_g molecular parameters [10], the largest Franck-Condon factors were predicted for transitions from $v'=4$ to $v^+=0$ of the $C\ ^2\Pi_{3/2u}$ ion state and to $v^+=47$ of $A\ ^2\Sigma^+_{1/2u}$. This leads to calculated photoelectron energies of 2.59 and 2.90 eV, respectively, and leaves little doubt that the measured photoelectron peak at 2.53 eV arises from an ionization process that leaves Xe_2^+ in the C-state. This conclusion can also be reached with the correlation diagram in Fig. 1.

While the higher-energy component at 2.71 eV is too low to involve the A state, the measurement agrees well P_{KE}=2.74 eV, derived by assuming that the ion core involved is $B\ ^2\Pi_{3/2g}$. We believe, therefore, that the experimentally observed doublet is a result of a perturbation that gives the 2_g Rydberg state mixed core character. The symmetry of the second ion core suggests that the 2_g perturber must dissociate to $Xe(^1S_0)$+Xe*$(5d)$. The most probable candidates are deduced from Fig. 2 as the 2_g state that dissociates to either $Xe(^1S_0)$+Xe* $5d[7/2]_4^0$ at 80 197.16 cm^{-1} or $Xe(^1S_0)$+Xe* $5d[3/2]_2^0$ at 80 323.28 cm^{-1} [9].

Dehmer, Pratt, and Dehmer reported a PE spectrum for the (2,0) band of this electronic transition and make the same molecular ion-core assignments [15]. In addition, they observed a third peak at $P_{KE} \approx 2.45$ eV. That they attributed to ionization from atomic Xe* $6p[5/2]_2$, which seems reasonable given that the 2_g Rydberg state has been found to be partially predissociated [10].

2. The 1_g Rydberg state

Spectral analyses of the $1_g \leftarrow 0_g^+$ transition in region III showed that the excited Rydberg state has a dissociation energy reminiscent of the A ion core ($D_e' \approx 2616$ cm^{-1} [37]). However, the correlation diagram predicts 1_g to be built upon Xe_2^+ $C\ \Pi_{3/2u}$ like the 2_g state in this vicinity. Since the excited state is strongly predissociated, the measured kinetic energy of P_{KE}=2.47 eV from the PE spectrum obtained by exciting the $1_g(v'=26) \leftarrow 0_g^+(v''=0)$ transition at 78 867.7 cm^{-1} [Fig. 8(a)] does not agree with those determined from Franck-Condon factor calculations using the C core (P_{KE}=2.57 eV) or the A core (ρ_{KE}=2.90 eV). However, the measurement does agree with that expected if the photoelectrons originate from Xe* $6p[5/2]_3$ at 78 403.562 cm^{-1} [9]. While it is possible that the REMPI transition actually involves the uncharacterized 1_g state, which dissociates to $Xe(^1S_0)$+Xe* $6p[3/2]_1$ at 78956.538 cm^{-1} [9], and is predicted to be built on $A\ ^2\Sigma^+_{1/2u}$, more likely, the entire manifold of 1_g states will have to be considered together to understand the spectroscopy completely [25].

The CIS spectrum in Fig. 8(b) recorded by setting the pass energy of the spectrometer to 2.47 eV shows both the $1_g \leftarrow {}_g^+$ and $2_g \leftarrow 0_g^+$ transitions, while that obtained using P_{KE}=2.53 eV [Fig. 8(c)] shows only the $2_g \leftarrow 0_g^+$ transition cleanly. This demonstrates the promise that the CIS tech-

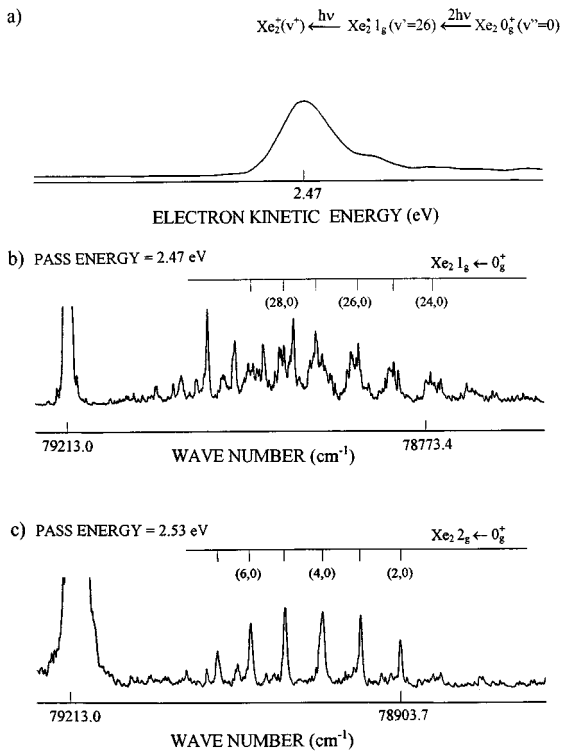

FIG. 8. (a) PE spectrum for the Xe_2 $1_g(v'=26) \leftarrow 0_g^+(v'=0)$ two-photon transition at 78 867.7 cm^{-1} in region III. (b) CIS spectrum obtained by setting the pass energy of the photoelectron spectrometer to 2.47 eV and frequency scanning the uv laser. Vibrational assignments for the Xe_2 $1_g \leftarrow 0_g^+$ two-photon transitions are those reported in Ref. [37]. (c) CIS spectrum obtained by setting the pass energy of the photoelectron spectrometer to 2.53 eV and frequency scanning the uv laser. Vibrational assignments for the Xe_2 $2_g \leftarrow 0_g^+$ two-photon transitions are those reported in Ref. [10].

nique holds for doing core- *and* frequency-resolved spectroscopy.

D. Region IV

The strongest feature in region IV is a (0,0) band at 78 016 cm^{-1} that has been assigned to a $2_g \leftarrow 0_g^+$ transition [10]. The shallow excited state ($D_e' = 300.2$ cm^{-1}) dissociates to $Xe(^1S_0) + Xe^*\ 6p[5/2]_2$. The resultant photoelectron spectrum shows a single peak at $P_{KE} = 2.47$ eV. Here energy calibration was based on PE spectra involving the Xe* $6p[5/2]_2 \leftarrow Xe(^1S_0)$ two-photon resonance.

Ionizing $2_g(v'=0)$ is calculated to leave Xe_2^+ in either $A\ ^2\Sigma_{1/2u}^+(v^+=51)$ or $C\ ^2\Pi_{3/2u}(v^+=0)$. The corresponding electron energies were derived using Eq. (2) to be 2.70 and 2.41 eV, respectively. This strongly supports a $C\ ^2\Pi_{3/2u}$ ion-core assignment for the 2_g Rydberg state, as predicted by Fig. 1.

The same core assignment was put forth by Dehmer, Pratt, and Dehmer based on a photoelectron feature at $P_{KE} \approx 2.4$ eV [15]. In their spectrum, however, a second weaker higher-energy peak ($P_{KE} \approx 2.5$ eV) was resolved, which they assigned to $B\ ^2\Pi_{3/2g}$. This unexpected result is again attributed to homogeneous interactions. We propose on the basis of energetics that the perturber is the 2_g state that dissociates to $Xe(^1S_0) + Xe^*\ 5d[7/2]_4^o$.

E. Regions V and VI

Molecular PE spectra in these regions were calibrated against atomic photoelectron data recorded for the Xe* $6p[5/2]_2 \leftarrow Xe(^1S_0)$ two-photon transition. The 0_g^+ state in region V, which dissociates to $Xe(^1S_0) + Xe^*\ 6p[5/2]_2$, and the 1_g state in region VI, which dissociates to $Xe(^1S_0) + Xe^*\ 6p[1/2]_1$, are both deep ($D_e' = 3470.4$ and 4701 cm^{-1}, respectively [10]). This is not unexpected since both levels are predicted to be built on Xe_2^+ $A\ ^2\Sigma_{1/2u}^+$ (Fig. 1). These ground-state ion-core assignments are now unambiguously confirmed in this work because when the $0_g^+(v'=32) \leftarrow 0_g^+(v''=0)$ transition at 77 586.7 cm^{-1} and the $1_g(v'=43) \leftarrow 0_g^+(v''=0)$ transition at 77 017.4 cm^{-1} were excited, the large resultant electron kinetic energies ($P_{KE} = 3.12$ and 3.10 eV, respectively) immediately show that Xe_2^+ was produced in an electronic level that lies much lower than the adiabatic IP of any excited state [19]. The CIS spectrum that reproduces the band systems in these spectral regions is presented in Fig. 9.

Based on Franck-Condon considerations, however, Xe_2^+ should be formed in high vibrational levels of $A\ ^2\Sigma_{1/2u}^+$ ($v^+ = 52$ for region V and $v^+ = 43$ for region VI), leading to photoelectrons with $P_{KE} \approx 2.6$ eV. The differences between these predictions and the experimental measurements are substantial. It should be appreciated, however, that Franck-Condon intensity is distributed over a wide range of v^+ lev-

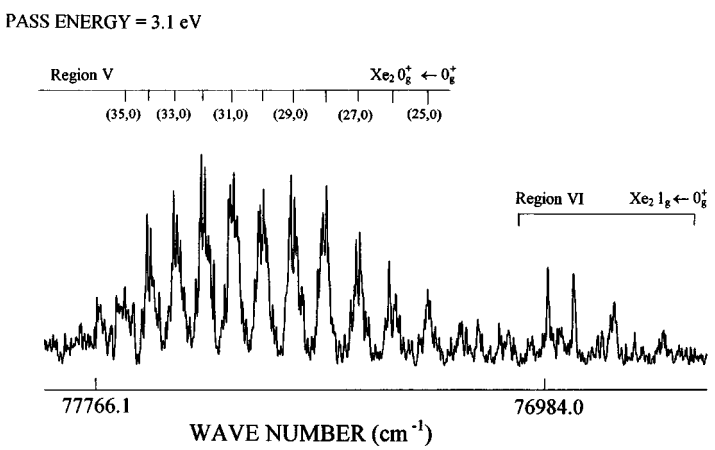

FIG. 9. CIS spectrum obtained by setting the pass energy of the photoelectron spectrometer to 3.1 eV and frequency scanning the uv laser in regions V and VI. Vibrational assignments for the Xe_2 $0_g^+ \leftarrow 0_g^+$ two-photon transition in region V are those reported in Ref. [10].

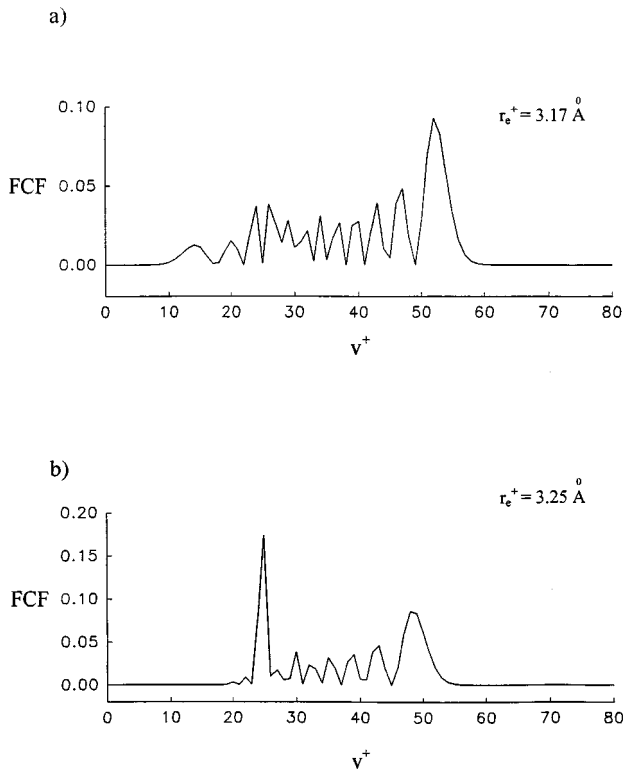

FIG. 10. (a) Plot of the $|\langle v^+|v'=32\rangle|^2$ Franck-Condon factors (FCF) for the Xe_2 $0_g^+(v'=32)\leftarrow 0_g^+(v''=0)$ two-photon transition in region V, as a function of the Xe_2^+ A-state vibrational quantum number v^+. The equilibrium bond length of the Rydberg state was set to 3.21 Å, while the ionic A-state equilibrium internuclear separation was $r_e^+=3.17$ Å. (b) Plot of the $|\langle v^+|v'=32\rangle|^2$ FCFs for the Xe_2 $0_g^+(v'=32)\leftarrow 0_g^+(v''=0)$ two-photon transition in region V, as a function of the Xe_2^+ A-state vibrational quantum number v^+. Here the equilibrium bond length of the Rydberg state was again set to 3.21 Å, but the ionic A-state equilibrium internuclear separation was increased to $r_e^+=3.25$ Å.

els in a complex way, which is not too surprising given the highly oscillatory nature of the Rydberg wave functions excited in the (2+1) REMPI process. This is illustrated in Fig. 10(a) for the transition in region V. Furthermore, small changes in the relative position of the ion ground-state potential-energy curve with respect to the Rydberg state can lead to large changes in the Frank-Condon factor intensity distribution [Fig. 10(b)]. Therefore, the uncertainty in the Rydberg and ion-state equilibrium bond lengths, both of which are not known from rotationally resolved spectra, could account, in small part, for the disagreements.

In addition and/or alternatively, the observations may be indicative of non-Franck-Condon behavior. While this phenomenon is not unprecedented it is also not well understood [38,39]. Possible causes for a Franck-Condon breakdown include kinetic-energy- and bond-length dependent excited-state dipole matrix elements, v^+-dependent electron angular distributions, perturbations, and autoionization. At this time, however, the relative importance of each probable cause can only be speculated. Vibronically resolved PE spectra will be required to investigate this matter further.

IV. CONCLUSIONS

The goal of this paper was to use photoelectron spectroscopy to establish the dominant molecular ion-core identities of the gerade Rydberg states of Xe_2 that dissociate to $Xe(^1S_0)+Xe^*(6p,5d)$. Where comparisons could be made, our conclusions were found to agree with those in the literature, but the scope of our work is more comprehensive.

In most instances, the ion-core assignments also agree with those predicted using correlation diagrams constructed from angular momentum arguments. At best, however, the photoelectron spectrum of a strongly predissociated molecular state can only yield the identity of the resultant excited atomic product. Furthermore, it is clear that excited-state interactions for Xe_2 are very important and must be considered for a complete understanding of the (2+1) REMPI spectra and associated photoelectron data.

As demonstrated by Dehmer, Pratt, and Dehmer [15], more information can be derived from PE spectra having better energy resolution. As noted above, by employing a smaller diameter aperture, the resolving power of our photoelectron spectrometer could be improved by a factor greater than 2. To achieve this improvement more effort will have to be made to optimize the dimer composition in the jet. The photoelectron techniques described here will help in the interpretation of new (2+1) REMPI-TOF spectra recently obtained for the higher-lying Xe_2 excited states dissociating to $Xe(^1S_0)+Xe^*(5d)$ and other asymptotic limits near the ionization limits of the molecule. That work will be the subject of future work [40].

ACKNOWLEDGMENTS

Financial research support from the Natural Sciences and Engineering Research Council of Canada and the Academic Development Fund of the University of Western Ontario is gratefully acknowledged. The authors thank John Vanstone for his continuing excellent technical help and Dr. Mike Bancroft for his comments concerning the manuscript.

[1] J. W. C. Johns, *A Specialist Periodical Report, Molecular Spectroscopy 2* (The Chemical Society, London, 1974), p. 513.
[2] D. J. Trevor, J. E. Pollard, W. D. Brewer, S. H. Southworth, C. M. Truesdale, D. A. Shirley, and Y. T. Lee, J. Chem. Phys. **80**, 6083 (1984).
[3] D. E. Freeman, K. Yoshino, and Y. Tanaka, J. Chem. Phys. **61**, 4880 (1974).
[4] R. S. Mulliken, J. Chem. Phys. **52**, 5170 (1970).
[5] G. Herzberg, *Spectra of Diatomic Molecules* (van Nostrand, Princeton, 1950).
[6] W. R. Wadt, J. Chem. Phys. **68**, 402 (1978).
[7] W. C. Ermler, Y. S. Lee, K. S. Pitzer, and N. W. Winter, J. Chem. Phys. **69**, 976 (1978).
[8] M. Daskalopoulou, H.-U. Böhmer, and S. D. Peyerimhoff, Z. Phys. D **15**, 161 (1990).
[9] C. E. Moore, *Atomic Energy Levels*, Natl. Bur. Stand.

(U.S.) Circ. No. 467 (U. S. GPO, Washington, DC, 1971), Vol. III.
[10] S. S. Dimov, J. Y. Cai, and R. H. Lipson, J. Chem. Phys. **101**, 10 313 (1994).
[11] S. S. Dimov, X. K. Hu, D. M. Mao, and R. H. Lipson, Chem. Phys. Lett. **239**, 332 (1995).
[12] X. K. Hu, D. M. Mao, S. S. Dimov, and R. H. Lipson, Chem. Phys. **201**, 557 (1995).
[13] P. M. Dehmer and J. L. Dehmer, J. Chem. Phys. **67**, 1774 (1977).
[14] P. M. Dehmer and J. L. Dehmer, J. Chem. Phys. **68**, 3462 (1978).
[15] P. M. Dehmer, S. T. Pratt, and J. L. Dehmer, J. Phys. Chem. **91**, 2593 (1987).
[16] R. G. Tonkyn and M. G. White, J. Chem. Phys. **95**, 5582 (1991).
[17] Y. Lu, T. Matsui, K. Tanaka, K. Ito, T. Hayaishi, and Y. Morioka, J. Phys. B **25**, 5101 (1992).
[18] Y. Lu, Y. Morioka, T. Matsui, T. Tanaka, H. Yoshii, R. I. Hall, T. Hayaishi, and K. Ito, J. Chem. Phys. **102**, 1553 (1995).
[19] R. I. Hall, Y. Lu, Y. Morioka, T. Matsui, T. Tanaka, H. Yoshii, T. Hayaishi, and K. Ito, J. Phys. B **28**, 2435 (1995).
[20] S. L. Anderson, Adv. Chem. Phys. **82**, 177 (1992).
[21] S. T. Pratt, P. M. Dehmer, J. L. Dehmer, and E. F. McCormack, Comments At. Mol. Phys. **28**, 259 (1993).
[22] J. K. Ku and D. W. Setser, J. Chem. Phys. **84**, 4304 (1986).
[23] S. S. Dimov, R. H. Lipson, T. Turgeon, J. A. Vanstone, P. Wang, and D. S. Yang, J. Chem. Phys. **100**, 8666 (1994).
[24] F. Spiegelmann, F. X. Gadea, and M. C. Castex, Chem. Phys. **145**, 173 (1990).
[25] E. Audouard and F. Spiegelmann, J. Chem. Phys. **94**, 6102 (1991).
[26] G. J. Lapeyre, J. Anderson, P. L. Gobby, and J. A. Knapp, Phys. Rev. Lett. **33**, 1290 (1974).
[27] E. W. Plummer, T. Gustafsson, W. Gudat, and D. E. Eastman, Phys. Rev. A **15**, 2339 (1977).
[28] P. Morin, M. Y. Adam, I. Nenner, J. Delwiche, M. J. Hubin-Franskin, and P. Lablanquie, Nucl. Instrum. Methods **208**, 761 (1983).
[29] R. N. Compton, J. C. Miller, A. E. Carter, and P. Kruit, Chem. Phys. Lett. **71**, 87 (1980).
[30] J. C. Miller and R. N. Compton, Chem. Phys. Lett. **93**, 453 (1982).
[31] K. Sato, Y. Achiba, and K. Kimura, J. Chem. Phys. **80**, 57 (1984).
[32] P. R. Blazewicz, X. Tang, R. N. Compton, and J. A. D. Stockdale, J. Opt. Soc. Am. B **4**, 770 (1987).
[33] K. T. Lu and U. Fano, Phys. Rev. A **2**, 81 (1970).
[34] K. Kimura, in *Photodissociation and Photoionization*, Advances in Chemical Physics Vol. 60, edited by K. P. Lawley (Wiley, Chichester, 1985), p. 161.
[35] J. Tellinghuisen and S. D. Henderson, Chem. Phys. Lett. **91**, 447 (1982).
[36] R. H. Lipson and K. J. Jordan, J. Phys. Chem. **97**, 13 557 (1993).
[37] R. H. Lipson, A. R. Hoy, and E. Chan, J. Chem. Phys. **90**, 4664 (1989).
[38] S. T. Pratt, E. D. Poliakoff, P.M. Dehmer, and J. L. Dehmer, J. Chem. Phys. **78**, 65 (1983).
[39] S. T. Pratt, P. M. Dehmer, and J. L. Dehmer, Chem. Phys. Lett. **105**, 28 (1984), and references therein.
[40] X. K. Hu, D. M. Mao, S. S. Dimov, and R. H. Lipson (unpublished).